ELSEVIER

Physics of the earth and Planetary Interiors 123 (2001) 129-149

PHYSICS OF THE EARTH AND PLANETARY INTERIORS

www.elsevier.com/locate/pepi

Local earthquake tomography between rays and waves: fat ray tomography

Stephan Husen*, Edi Kissling

Institute of Geophysics, ETH Hoenggerberg, CH8093 Zurich, Switzerland

Abstract

The limitations of ray-based forward solutions in seismic tomography are theoretically well known. To correctly represent the physical forward problem in seismic tomography, application of full three-dimensional (3D) wave theory would be required. Up to now this is not possible for the size of a typical local earthquake study. With the concept of fat rays resembling the waves Fresnel volume, a more complete, physically consistent and accurate solution to the forward problem is available. In this paper we present an approach to include fat rays in local earthquake tomography, called FATOMO. The comparative study with synthetic data and inversion results with FATOMO and a ray-based approach to local earthquake tomography, SIMULPS, reveals new insights into the role of resolution and model parameterization in local earthquake tomography. Intuitively expected effects of fat rays on resolution estimates such as higher node sampling values and lower resolution diagonal element values for wider fat rays can be seen in the results. For ideal model parameterization, differences between fat ray and ray tomography are small. Our results document, however, that the influence of model parameterization is less critical for fat ray tomography than for ray tomography. ' 2001 Elsevier Science B.V. All rights reserved.

Keywords: Seismic Tomography, Fat Rays, Finite-Difference Modelling, Solution Quality

1. Introduction

Precision of the solution to the forward problem is of great importance in seismic tomography since both sides of the linearized matrix Eq. (1) describing the inverse problem are affected:

$$\boldsymbol{d} = \boldsymbol{A}\boldsymbol{m} + \boldsymbol{e} \quad (1)$$

where $\boldsymbol{d}$ denotes the vector of travel time residuals, $\boldsymbol{A}$ the matrix of partial derivatives, $\boldsymbol{m}$ the vector of model adjustments, and $\boldsymbol{e}$ the error vector. The vector of travel time residuals $\boldsymbol{d}$ on the left-hand side of Eq. (1) directly depends on the precision and accuracy of the employed forward scheme, since residuals are defined as the differences between observed and calculated travel times. On the right-hand side of Eq. (1) the matrix $\boldsymbol{A}$ contains the partial derivatives of travel times with respect to model parameters and, hence, equally depends on precision and accuracy of the forward scheme to calculate travel times and ray paths. Small differences in ray paths due to the use of different ray tracers will result in different model partial derivatives, which may lead to a different solution of Eq. (1). Consequently, the solution to the forward problem must not only provide accurate travel times but also accurate travel paths for seismic waves. Two additional requirements have to be met for the solution to the forward problem. First, it must be fast since thousands of travel times and partial derivatives need to be calculated at each iteration. Second, it must be robust in the presence of strong velocity heterogeneities.

* Corresponding author. Fax: ++41-1-6331065.
E-mail addres: stephan@tomo.ig.erdw.ethz.ch (S.Husen)

0031-9201/007$ - see front matter
PII: S0031-9201(00)00206-5

Forward solutions based on a ray theoretical approach have been used in local earthquake tomography since its beginning. These solutions include full or approximate 3D ray tracing by bending or shooting. The pseudo-bending approximate ray tracing (ART-PB) method proposed by Um & Thurber (1987) and implemented in the widely used SIMULPS 3-D inversion algorithm (Evans et al., 1994) represents an approximate 3D ray tracer with additional pseudo bending-type ray pertubations. Um & Thurber (1987) and Eberhart-Phillips (1990) pointed out that ART-PB is only accurate for ray lengths up to 80 km. Virieux (1991) and Virieux and Farra (1991) presented a full 3D shooting algorithm based on paraxial ray tracing. This method has been used in local earthquake tomography by Le Meur et al. (1997) and Ghose et al. (1998) and implemented in SIMULPS by Haslinger (1999). Ray tracing is very efficient to find travel times and ray paths simultaneously, but all ray tracing schemes share the same drawback: they offer no guarantee that the global minimum travel-time is found.

With increasing computer power a new method of calculating travel times has become available for tomography studies that solves the eikonal equations by finite difference (FD) methods (Vidale, 1988, 1990; Podvin & Lecomte, 1991; Hole & Zelt, 1995). Solving the eikonal equations directly guarantees that the global minimum travel time is found. To compute partial derivatives, however, FD-based tomography studies still use ray paths which are normally computed by following the steepest gradient in the travel time field from source to the receiver or vice versa (Podvin & Lecomte, 1991; Hole, 1992). Hence, these approaches could still be considered as belonging to the class of ray-based tomography, except that they could possibly find first arrivals normally not found by ray-based tomography.

To correctly represent the physical forward problem in local earthquake tomography, the application of full 3D wave theory would be required. Wave-theoretic or wave-equation tomography requires the forward and backward propagation of the full seismic wavefield (Vasco, Peterson, & Majer, 1995). This problem is usually formulated in the frequency-wavenumber domain under the title of diffraction tomography (Woodward (1992), and references therein). Modelling even the full acoustic wavefield is still a computationally intensive task. It has been sucessfully implemented in 2D cross-borehole tomography (e.g. Luo & Schuster, 1991; Vasco & Majer, 1993; Vasco, Peterson, & Majer, 1995). For the size of a typical local earthquake tomography study and in 3D, however, this has not been possible due to computational requirements. For a more thorough discussion of the standard solutions to the forward problem in seismic tomography see Thurber and Kissling (2000).

In this paper we present a new approach to the solution of the forward problem in local earthquake tomography that combines elements of both ray- and wave theoretical approaches. Travel times are calculated using finite difference (FD) modelling of the eikonal equations (Podvin & Lecomte, 1991) and travel paths and partial derivatives are computed using fat rays as described below. Such fat rays resemble the first Fresnel volume of a wave for a specific frequency. We also extend the ray-independent approach to the problem of earthquake location by implementing a grid-search algorithm. With the use of a simple synthetic test case we investigate the influence of our new forward solution on inversion results and on resolution estimates. A second test using synthetic data computed for the source-receiver distribution of a real experiment in northern Chile is used to compare inversion results and resolution estimates obtained by the fat ray approach (FATOMO; Husen, 1999) to those obtained by a ray-based approach (SIMULPS; Thurber, 1983 and Eberhart-Phillips, 1990).

2. Fat Ray Concept

The idea of using rays of non-zero width to bridge the gap between rays and waves dates back to Hagedoorn (1954). He tried to relate rays and waves by introducing the idea of a beam width, which is defined as the region falling within the first Fresnel volume. The first Fresnel volume of a seismic wave is defined as the innermost spatial region where constructive interference of seismic energy takes place. Hence, scattering from each point within the first Fresnel volume contributes constructively to the signal observed at a receiver. Travel times observed in the "real earth" reflect propagation of seismic energy in the first Fresnel zone. In doing seismic tomography, it would be "nice" to incorporate a greater degree of this reality.

Various attempts exist in the literature to compute Fresnel zones or volumes for bandlimited seismic

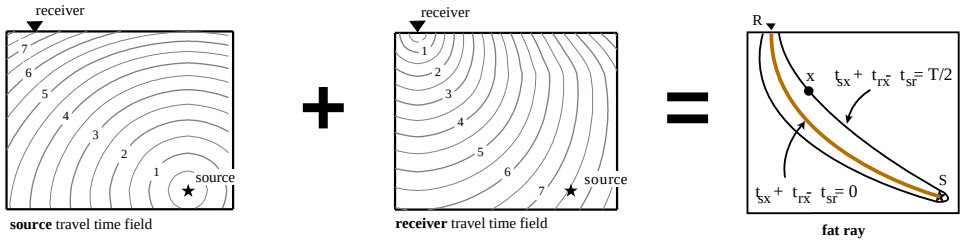

Fig.1 Schematic diagram of the fat ray concept. Both source and receiver travel time fields are computed using finite-difference modelling. Their summation is used to define a fat ray, given those points with a summed travel time less than $t_{sr} + T/2$ (t_{sr} = travel time source-receiver, T = dominant wave period).

travel times. They either use the Born or Kirchhoff approximation to compute Fréchet kernels or derivatives (Gelchinsky, 1985; Cardimona & Garmany, 1993; Stark & Nikolayev, 1993; Vasco & Majer, 1993; Marquering et al., 1999) or ray theory (Cerveny & Soares, 1992; Vasco et al., 1995; Pulliam & Snieder, 1998). Recently, Dahlen et al. (2000) presented a way to compute 3D Fréchet kernels using body wave ray theory in conjunction with the Born approximation. Pulliam & Snieder (1998) presented two methods to compute approximate Fresnel zones in inhomogeneous media, which are similar to our approach. They use ray perturbation theory and the network ray tracing method of Klimes & Kvasnicka (1994), respectively, to compute seismic travel times instead of a finite-difference algorithm as in our approach.

Reformulation of wave-equation tomography in the frequency-space domain (Woodward, 1992) reveals that monochromatic, scattered wavefields are back-projected along source-receiver wave paths, just as ray-based tomography distributes travel time delays over ray paths. Moreover, for the nondispersive case and a specific frequency bandwidth, wave paths can be approximated by band-limited ray paths or fat rays, which resemble the first Fresnel volume associated with that frequency band (Woodward, 1992). The computation of a single wave path requires forward and backward propagation of the acoustic seismic wavefield making it computationally rather intensive. On the other hand, with increasing computer power, FD modelling of the eikonal equations is relatively fast. The summation of both travel time fields, for the forward and the backward propagating waves, yields the fat ray (Fig. 1) representing the wave path from source to receiver. In our approach, we use the finite-difference algorithm of Podvin & Lecomte (1991) to compute travel time fields.

Cerveny and Soares (1992) defined the width of the Fresnel volume in terms of travel times t_{sx},t_{rx} between source or receiver respectively, and a point x within the Fresnel volume as (Fig. 1)

$$| t_{sx} + t_{rx} - t_{sr}| \leq T/2 \qquad (2)$$

where T is the dominant period of the seismic wave and t_{sr} the shortest travel time between source and receiver. Consequently, the width of a fat ray should be defined by the points satisfying the equality in Eq. 2 to correctly represent the first Fresnel volume (Fig. 1). For a dominant frequency of 10 Hz, for example, the ideal fat ray width should correspond to points having a 0.05 s travel time difference. Assuming a volume of uniform velocity of 5 km/s, this corresponds to a *minimum fat ray width* of 500 m in the vicinity of the source and receiver. Fig. 2 displays a fat ray representing a head wave in a simple two-layer model. As expected from the behavior of Fresnel zones, the fat ray tends to broaden in the area of higher velocity.

To implement fat rays in seismic tomography, we resample fat rays using cells defined on the grid used for the FD modelling (Fig. 2b). This grid, called forward or numerical grid, is needed to perform a stable computation of the travel time fields (Kissling et al., 2000). The grid spacing of the numerical grid must be small enough to correctly approximate the wave fronts and, therefore, it is also a good choice to discretize the fat rays. To correctly represent fat rays, grid spacing of the numerical grid must be smaller than the mini-

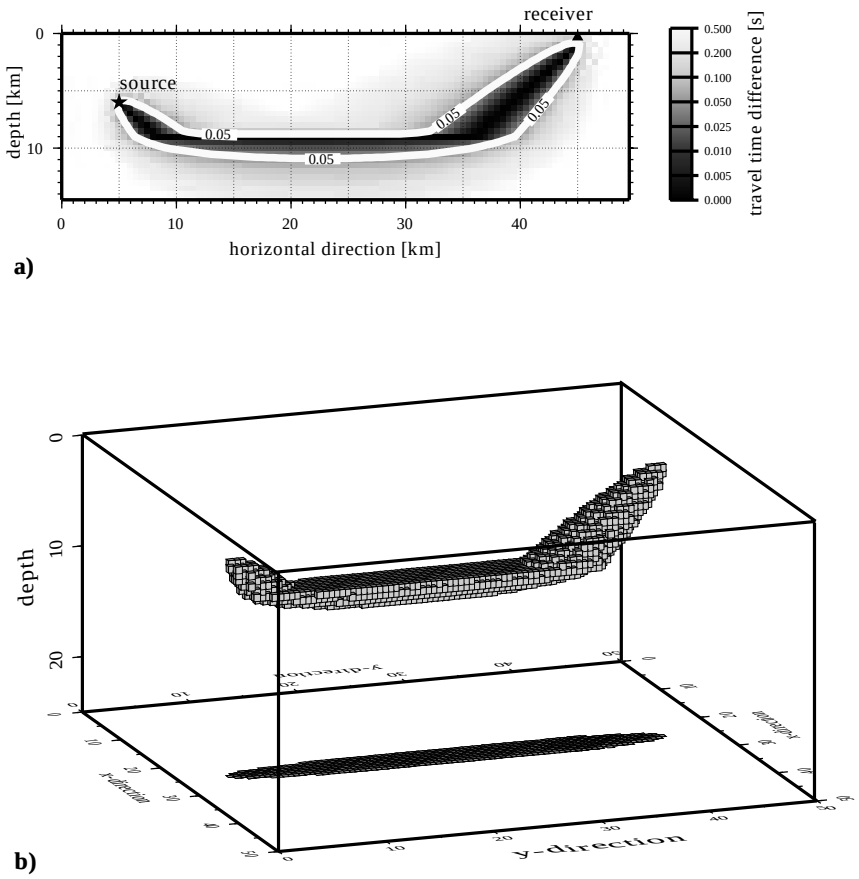

Fig. 2. Fat ray examples in a) 2D and b) 3D for a head wave in a simple two layered velocity model. The contour in a) denotes a fat ray width of 0.05

mum fat ray width. To compute the partial derivative of the travel time with respect to the *k*th model parameter, we need to know how much a fat ray is influenced by a certain model parameter.. In the case of a block model as inversion grid such as ours, this is simply that part of the fat ray located within the inversion cell associated with the *k*th model parameter (Fig. 3). Thus, the partial derivative with respect to the fractional slowness perturbation $\Delta u_k/u_k$ at *k*th model parameter becomes

$$\frac{\partial t}{\partial(\Delta u_k/u_k)} = -\frac{\mathrm{sum}_k}{\mathrm{vol}_{\mathrm{sr}}}\mathrm{tt}_{\mathrm{sr}} \qquad (3)$$

where sum_k denotes the number of numerical cells (volume) of the fat ray within the *k*th inversion cell (see Fig. 3), $\mathrm{vol}_{\mathrm{sr}}$ is the total number of numerical cells of the fat ray (total fat ray volume), and $\mathrm{tt}_{\mathrm{sr}}$ is the total travel time between source and receiver.

3. Earthquake Location

The coupling between seismic velocities and hypocenter locations in the inverse problem requires the relocation of earthquakes during the inversion process. To extend the ray-independent solution of the forward problem to the problem of earthquake location, we im-

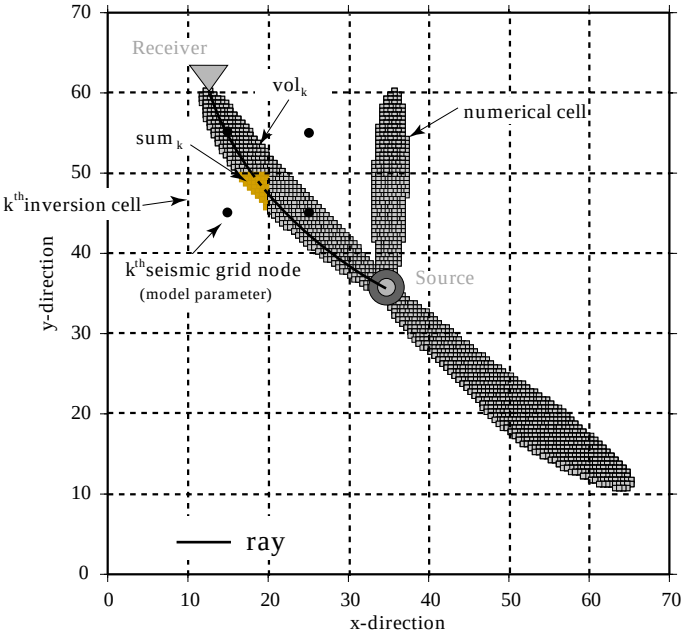

Fig. 3. Plan view of fat rays discretized by numerical cells. The shaded area represents that area of the fat ray, which is influenced by the velocity defined at the k-th seismic grid point. Black circles denote all seismic grid nodes, which influence the ray segment shown as dashed line. See text for further explanation.

plemented a grid-search algorithm. The computation of fat rays requires the calculation of the full travel time field for each receiver, so that from each point in the model, travel times to each station are available. Consequently, a grid search method for earthquake location is well suited for fat ray tomography. With grid search methods one tries to localize a global minimum of a misfit function by performing a direct search over the gridded parameter space. In the case of earthquake location, the misfit function depends on the four hypocentral parameters: the hypocentral coordinates and the origin time. This requires a temporal search over a range of possible origin times as well as a spatial search over a range of possible hypocentral coordinates (Sambridge & Kennett, 1986). In the case of well-locatable events and an appropriate initial reference model, which are necessary prerequisites to obtain reasonable and stable solutions to the coupled hypocenter-velocity model problem (Kissling et al., 1994), the best fitting origin time T_{org} for a particular grid point may be found by the formula (Nelson & Vidale, 1990):

$$T_{\text{org}} = \frac{1}{N}\sum_{N=1}^{N}(T_{\text{obs}_N} - T_{\text{calc}_N}) \quad (4)$$

where N is the number of observations, T_{obs} are the observed arrival times and T_{calc} are the calculated travel times. The grid point that yields the smallest residual is considered the best location.

In our approach, we perform the grid search on two grids: first on the coarse seismic grid and second on the fine numerical grid. In Fatomo the seismic grid is used to parameterize the velocity field (Kissling et al. this issue). The grid search starts at the grid point closest to the initial hypocenter location and covers a user-defined radius which should encompass several seismic grid nodes in each direction to ensure that the global minimum is included (Fig. 4a). For the second search, a box is set up with its center at the location of the lowest RMS value of the initial search with sides

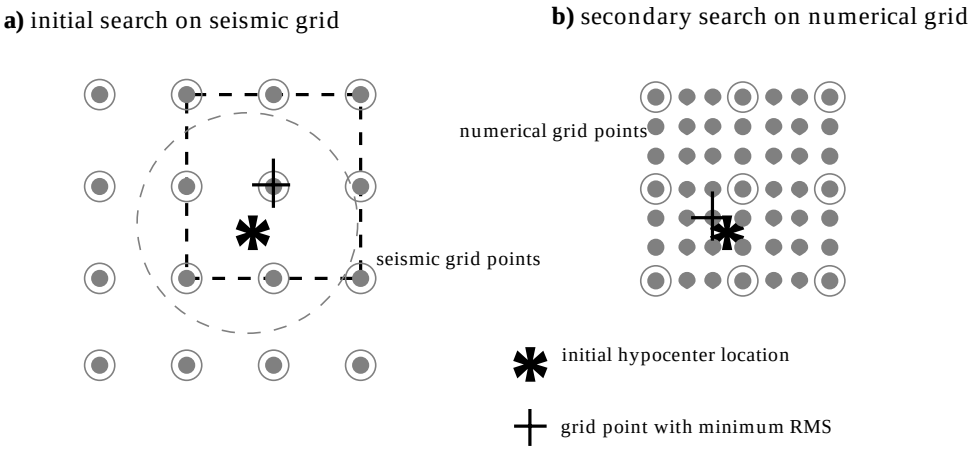

Fig. 4. Sketch of the different grids used in the grid search implemented in fat ray tomography. a) The initial search is performed on the coarse seismic grid. The dashed circle denotes the search radius. b) A second grid search is performed on the fine numerical grid with the minimum RMS location of the coarse search as its center.

defined by the surrounding seismic grid nodes (Fig. 4b). This second search is performed on the numerical grid, used for computation of travel times, which is 5 to 10 times smaller than the seismic grid. If in any of the searches the location with the minimum RMS value is at a search boundary, the grid is moved so that the minimum RMS location forms the new center, and the grid search is repeated. With the travel times already calculated for the fat ray computation, the implemented grid search approach provides not only a stable, but also a very fast and efficient method to relocate well-locatable events in the fat ray tomography algorithm.

A major advantage of grid search methods is the direct access to the misfit function in the area around the proposed hypocenter location (Fig. 5), which allows a more realistic estimation of the location accuracy. The accuracy of the proposed hypocenter location can be described by contours of constant confidence levels. Sambridge & Kennett (1986) presented an approach to compute such contours with the use of the chi-squared distribution with (n-4) degrees of freedom, where n is the number of data values. Analyzing such contours for a large set of events, however, is rather impractical. In our approach we assess the 95% confidence levels in each direction of the hypocenter location by determining those grid points which show a 2 sigma difference in the RMS value with respect to the RMS value at the hypocenter location. The 2 sigma value is defined by the mean travel time accuracy based on the observations weights. The ratio of the 95% confidence levels will give a crude approximation of the quality of the hypocenter solution, i.e., if the misfit function shows a more circular or a more ellipsoidal shape. Fig. 5 displays the misfit function for two example events of the synthetic data set described in the next section.

4. Tests of Fat Ray Tomography with Synthetic Data

A simple synthetic 3D-structure was used to test fat ray tomography and to investigate the influence of different fat ray widths on solution and resolution estimates. The latter is of special importance since available computer capacity often limits the size of the numerical grid. This implies that in some cases the minimum fat ray width cannot be as small as required by the dominant wave length. The synthetic structure used in this test consists of two velocity anomalies with ±15% velocity deviation (Fig. 6) embedded in a background model with a vertical velocity gradient. To generate sufficient ray coverage, 50 events at different depths and 25 stations are used (Fig. 6). Each event is observed at all stations, yielding 1250 observations. Synthetic travel times were calculated using

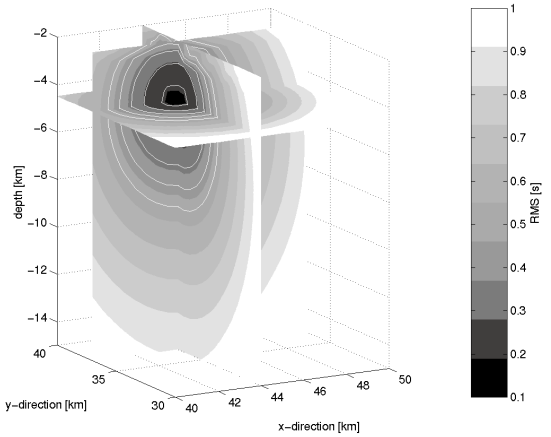

a) event 01: x = 44.0 km, y = 37.0 km, z = 4.5 km

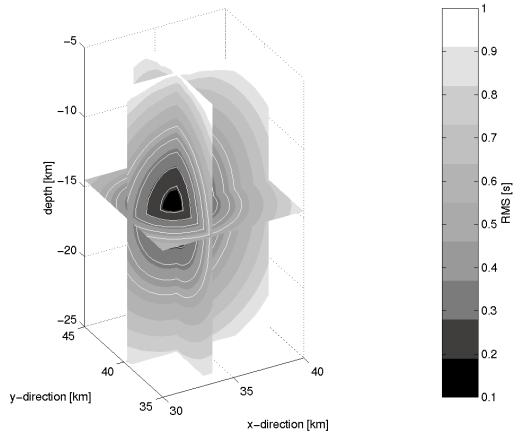

b) event 23: x = 33.5 km, y = 39.5 km, z = 18.5 km

Fig. 5. RMS volume (misfit function) of two example events as obtained by grid search. The hypocenter location is at the intersection of the thr shown from 0.2 s to 0.6 s at 0.1 s interval.

the FD forward solver of the eikonal equations (Podvin & Lecomte, 1991) with a gridspacing of 250 m. No noise was added to the travel times. Velocities in fat ray tomography are defined at grid points of the seismic grid, spaced 5 km apart with linear interpolation in between. To account for heterogeneous ray coverage, an additional block model, called the inversion grid, is used for the inversion (Kissling et al., 2000). In this test series, each inversion cell encompasses one seismic grid point.

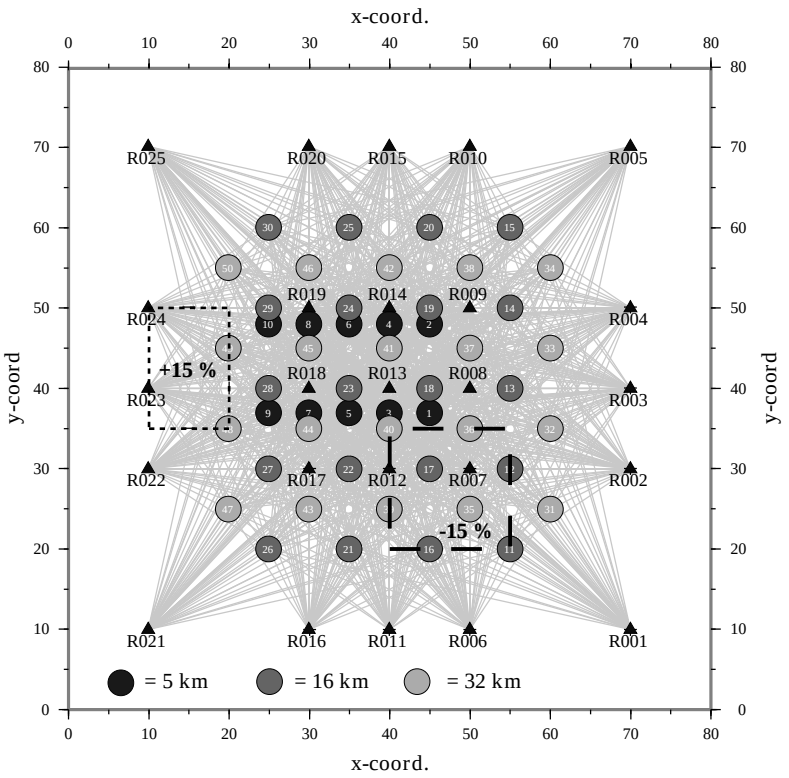

Fig. 6. Source (circles) and receiver (triangles) distribution used to test different fat ray widths. Grey lines connect source and receiver to display the ray distribution. Focal depths of the events are grey coded as indicated. Dashed lines show position of the two velocity anomalies located between 10 km and 20 km depth.

We test the effects of three different fat ray widths (corresponding to 0.04 s, 0.05 s, 0.07 s travel time difference) on the inversion results. Assuming an average velocity of 5.5 km/s, this corresponds to a minimum fat ray width of 440 m, 550 m, and 770 m. In the following, KHIT (number of fat rays per inversion cell) and RDE (diagonal element of the resolution matrix) are used to investigate the effects of different fat ray widths on resolution estimates. To avoid nonlinear path effects by the 3D-velocity inversion on the fat ray distribution, KHIT and RDE are shown after the first iteration in Figs. 7 and 8. The results of the inversion after 2 iterations are shown in Fig. 9. For more clarity, only two representative depth sections at 10.0 and 20.0 km depth are shown in Figs. 7-9.

As can be inferred from Fig. 7, KHIT shows higher values and a more homogenous distribution with increasing fat ray width. The effect is especially visible at greater depth due to higher velocities that increases fat ray width. This clearly documents the dependence of KHIT on the applied forward solution and model parameterization, complicating the use of KHIT for resolution assessment. On the other hand, the explicit dependence of KHIT on the forward solution makes it very useful for studying different forward solutions. The RDE in Fig. 8 exhibits decreasing values for increasing fat ray width, which is clearly visible, for example, at station R025. The region of uniform RDE in Fig. 8, however, is identical for all different fat ray widths.

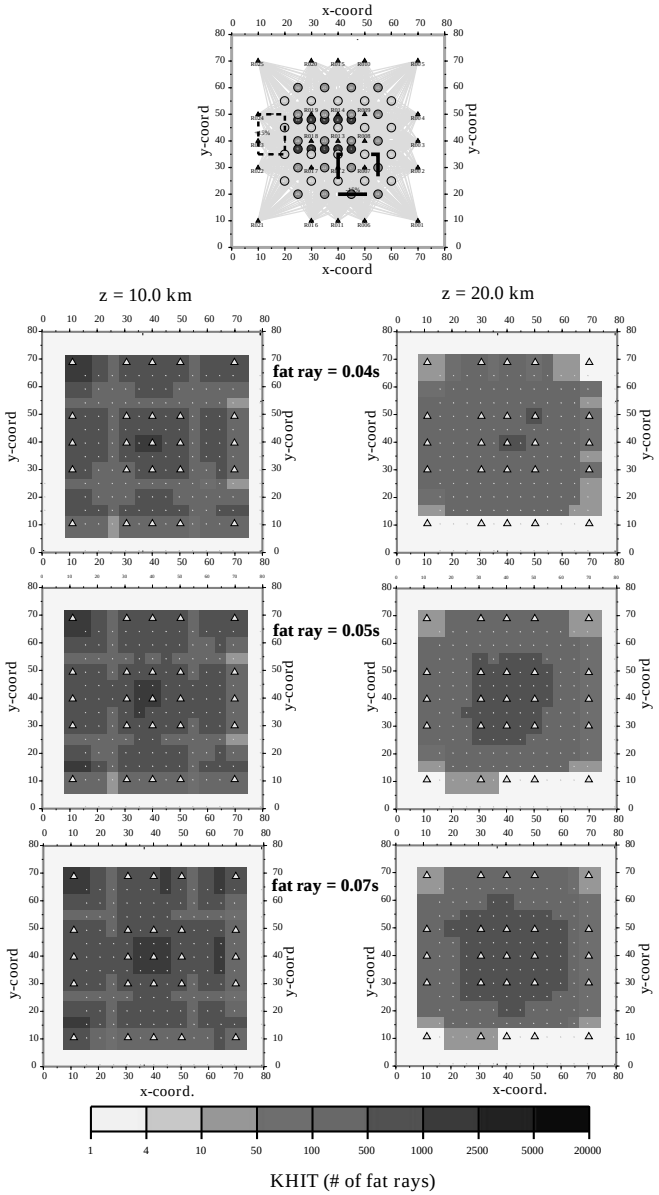

Fig. 7. KHIT values for inversion of synthetic data using the source-receiver distribution shown in Fig. 6 for different fat ray widths. Fat ray width increases from top to bottom. On top a plan view of the source-receiver and ray distribution is shown.

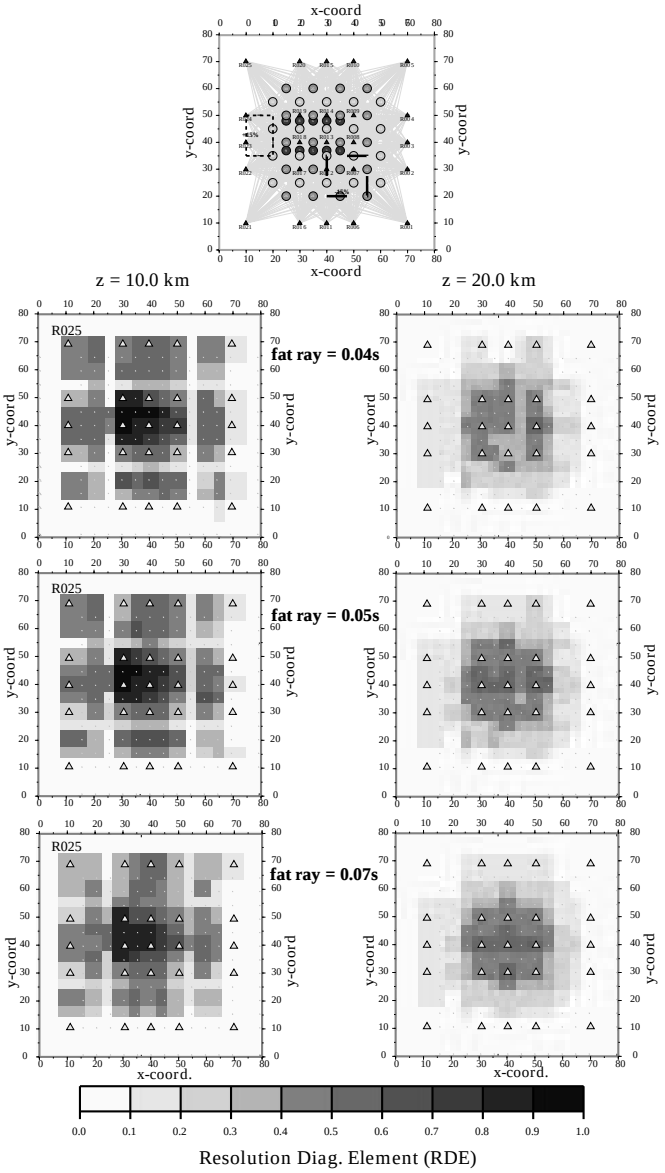

Fig.8. RDE values for inversion of synthetic data using the source-receiver distribution shown in Fig. 6 for different fat ray widths. Fat ray width increases from top to bottom. On top a plan view of the source-receiver and ray distribution is shown.

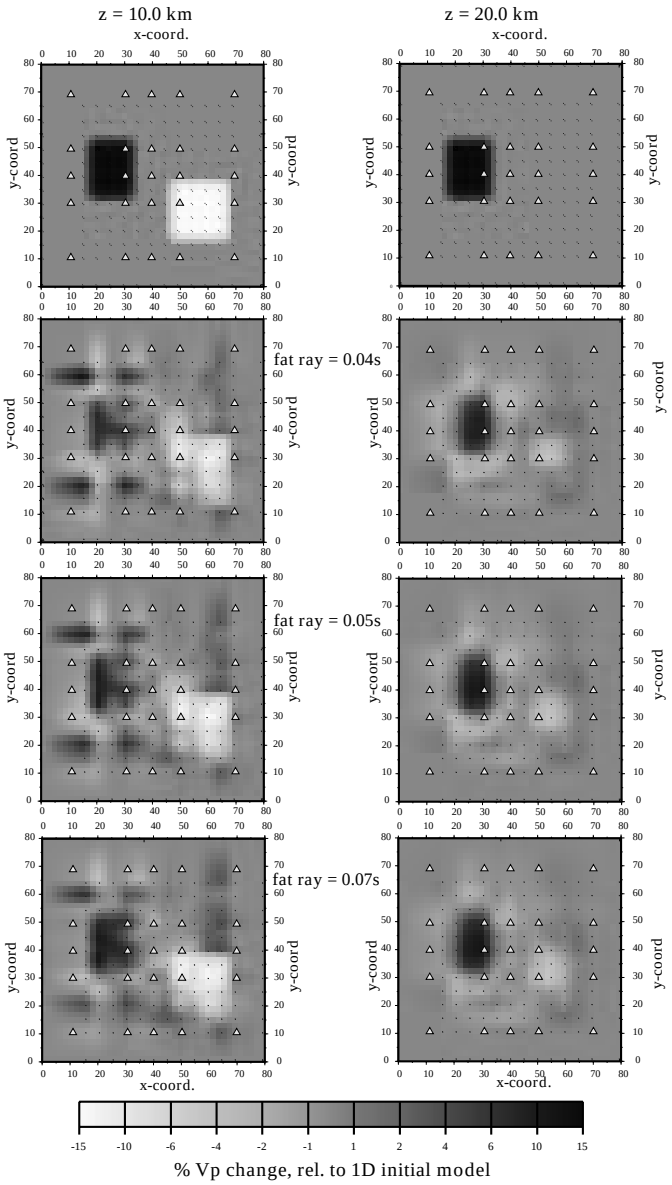

Fig. 9. Inversion results after 2 iterations of synthetic data set obtained with the source-receiver distribution shown in Fig. 6 for different fat ray widths. Fat ray width increases from top to bottom. On top the synthetic input model is shown.

Kissling (1988) and Haslinger et al. (1999) document that solution quality depends more on the uniformity than on absolute values of RDE. Therefore, no large differences in the solution are expected for different fat ray widths, which is confirmed by the inversion results (Fig.Fig. 9). Compared to the true model, all three solutions recover the synthetic structure at nearly the same level. Some smaller differences, however, can be observed. The image of the high velocity anomaly at 10.0 km depth is more patchy for the solution with 550 m and 440 m fat ray widths, which is similar (550 m) or less (440 m) than the numerical grid spacing of 500 m.

5. Comparing fat ray Tomography with ray tomography

To compare inversion results and resolution estimates of fat ray tomography with those of ray tomography, we used the geometry of the real data set of the CINCA experiment in the Antofagasta area, northern Chile (Husen et al., 2000). This data set consists of 789 well locatable local events recorded at a temporary network operating on- and offshore (Fig. 10). Synthetic travel times were calculated through the model shown in Fig. 11 using a 3D-shooting ray tracer (Vireux and Fara, 1991) and Gaussian noise was added. Ray tomography of this synthetic data set was performed using the SIMULPS software, which solves the forward problem by approximate 3D ray tracing with pseudo bending (Um & Thurber, 1987). Appropriate damping for velocities in ray tomography was determined to be 50 by analyzing trade-off curves between data and model variance (Eberhart-Phillips, 1986). Damping of the fat ray inversion depends on fat ray width and the size of the inversion cells (Kissling, this issue) and has been adjusted to 100. According to equation 2 and a dominant frequency of 6 Hz observed in the CINCA data set, the travel time difference for points within a fat ray was set to 0.09s. To avoid any effects caused by different model parameterizations, identical seismic and inversion grid spacing of 20 km was chosen for the fat ray and the ray tomography (Fig. 10). Numerical grid spacing used for FD modelling was 1 km.

Inversion results of the fat ray and ray tomography are shown in Fig. 11 for three selected horizontal depth sections. When compared to the true model, both inversion schemes show identical areas of good resolution, i.e. areas with good recovery of the true model, and areas of significant leakage problems. Fat ray tomography, however, shows a slightly better spatial recovery and more homogeneous amplitude recovery at 15 km and 35 km depth. Also, velocity smearing at 25 km depth is not as dominant as in ray tomography. On the other hand, ray tomography shows a higher sensivity in the border region of the resolved area, which results in higher amplitudes in these areas. Unfortunately, this applies for both true model recoverage and artefacts. RDE and KHIT for the layers shown in Fig. 11 are presented in Figs. 12 and 13, respectively. Compared to ray tomography, fat ray tomography yields higher absolute values and a more homogenous RDE distribution. For KHIT the opposite effect is observed (Fig. 12). Here, ray tomography shows larger areas of high KHIT, especially in the outer regions of the model.

At first glance, the similarities in the inversion results obtained by ray and fat ray tomography may come as a surprise, but one must keep in mind that in SIMULPS each ray segment is affected by all the surrounding grid points due to linear interpolation between the grid points (Fig. 3). Hence, with a lateral grid spacing of 20 km, each ray effectively influences a region 20 km in diameter. The diameter of a fat ray defining the area of influence is not constant and depends on velocity structure and source-receiver distance. We calculated the average effective fat ray diameter by dividing the fat ray volume by the corresponding ray length. For a fat ray width of 0.09 s and a total of 16070 rays we found an average effective fat ray diameter of 6 km. This is significantly smaller than the area of influence of 20 km in diameter determined for ray tomography. Hence, in this particular case the influence region of a ray is about three times larger then the average diameter of a fat ray. Since with KHIT one simply counts if a grid point is influenced by a ray or not, larger areas of high KHIT are expected in our synthetic test for ray tomography. The influence of the surrounding grid points on a ray segment is, of course, downweighted by the distance of the ray segment from the grid point. This damping of the influence on a ray segment with increasing distance from a grid point results in smaller RDE values for ray tomography than for fat ray tomography, where equal weight to a fat ray cell is given within the

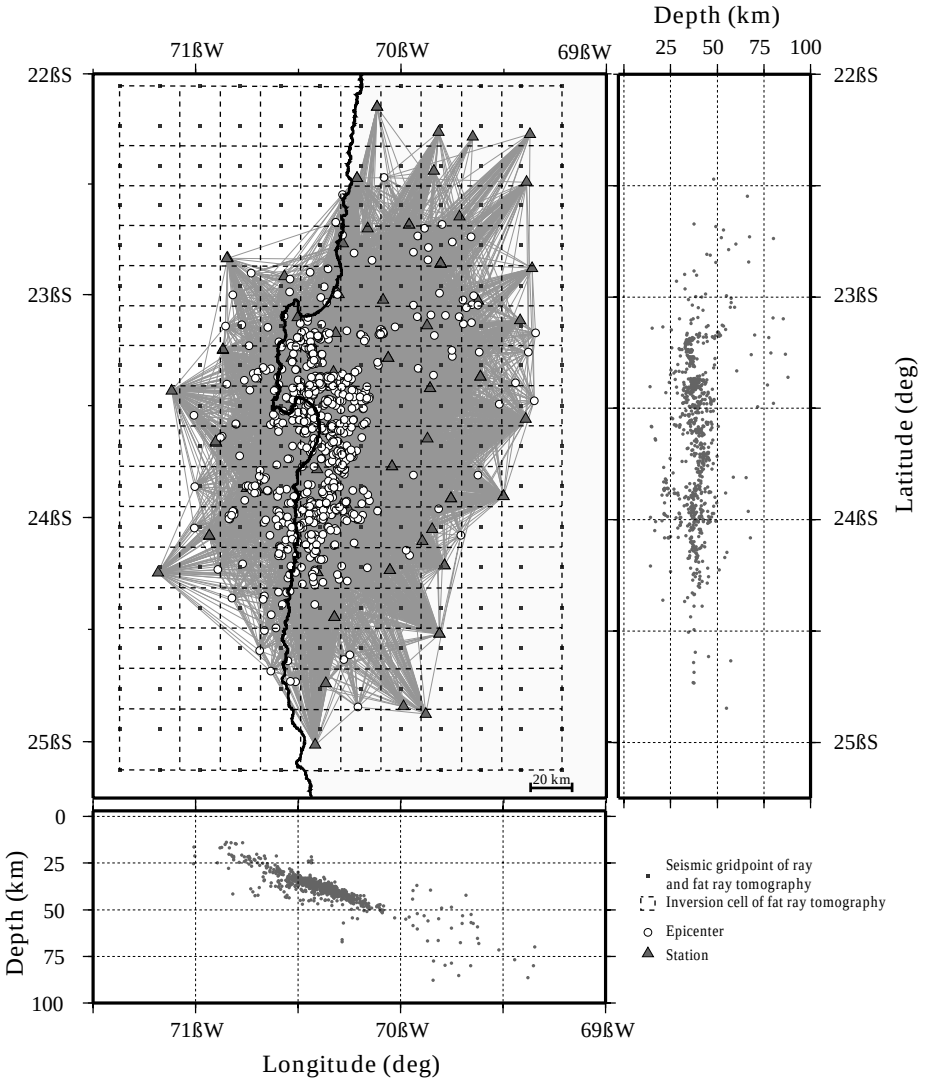

Fig. 10. Source (circles) and receiver (triangles) distribution of the real CINCA data set (Husen et al., 1999) used to compare fat ray and ray tomo raphy. Grey lines connect source and receiver to display the ray distribution. Seismic grid nodes of fat ray and ray tomography are shown by bla squares. Dashed lines show inversion cells used in the fat ray inversion.

fat ray volume. In SIMULPS, distribution of the travel time residual over adjacent grid nodes results in larger off-diagonal elements in the resolution matrix (Fig. 14). Consequently, velocity smearing is stronger for ray tomography than for fat ray tomography. Less velocity smearing not necessarily means that fat ray tomography has lower model uncertainties. Slightly better spatial recovery and more homogenous

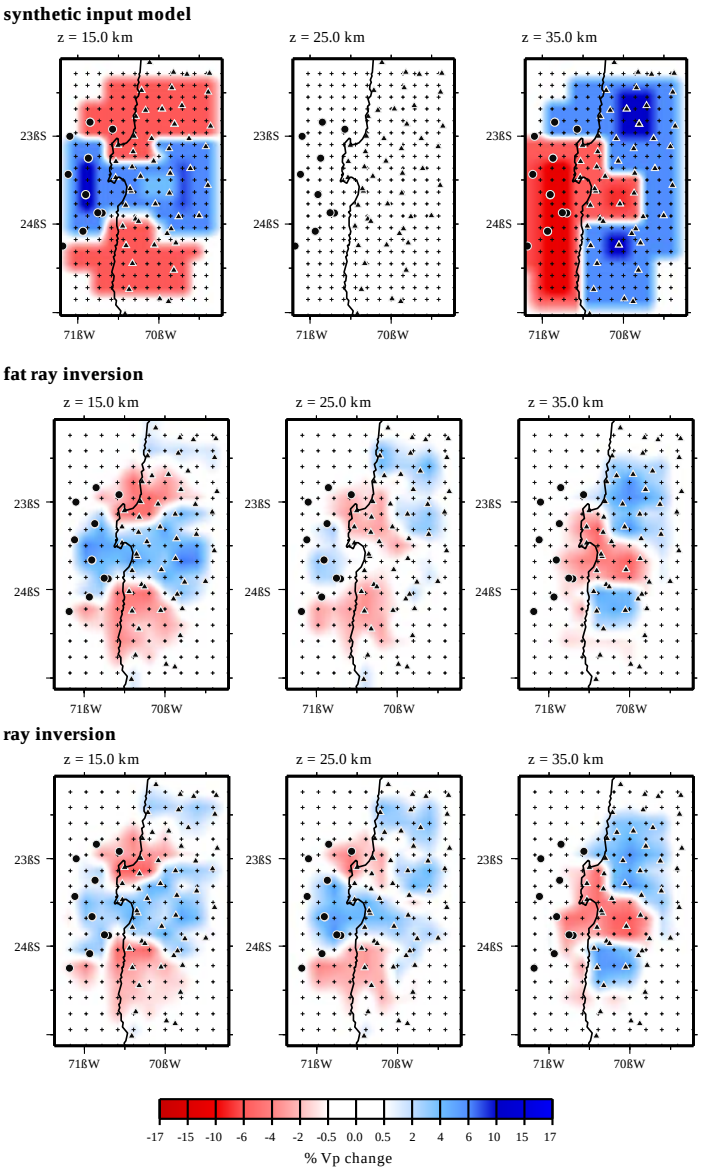

Fig.11. Synthetic input model (top) and inversion results after 2 iterations obtained by fat ray (middle) and ray inversion (bottom). Circles (offshore) and triangles mark stations (onshore). Crosses mark grid nodes defining velocities.

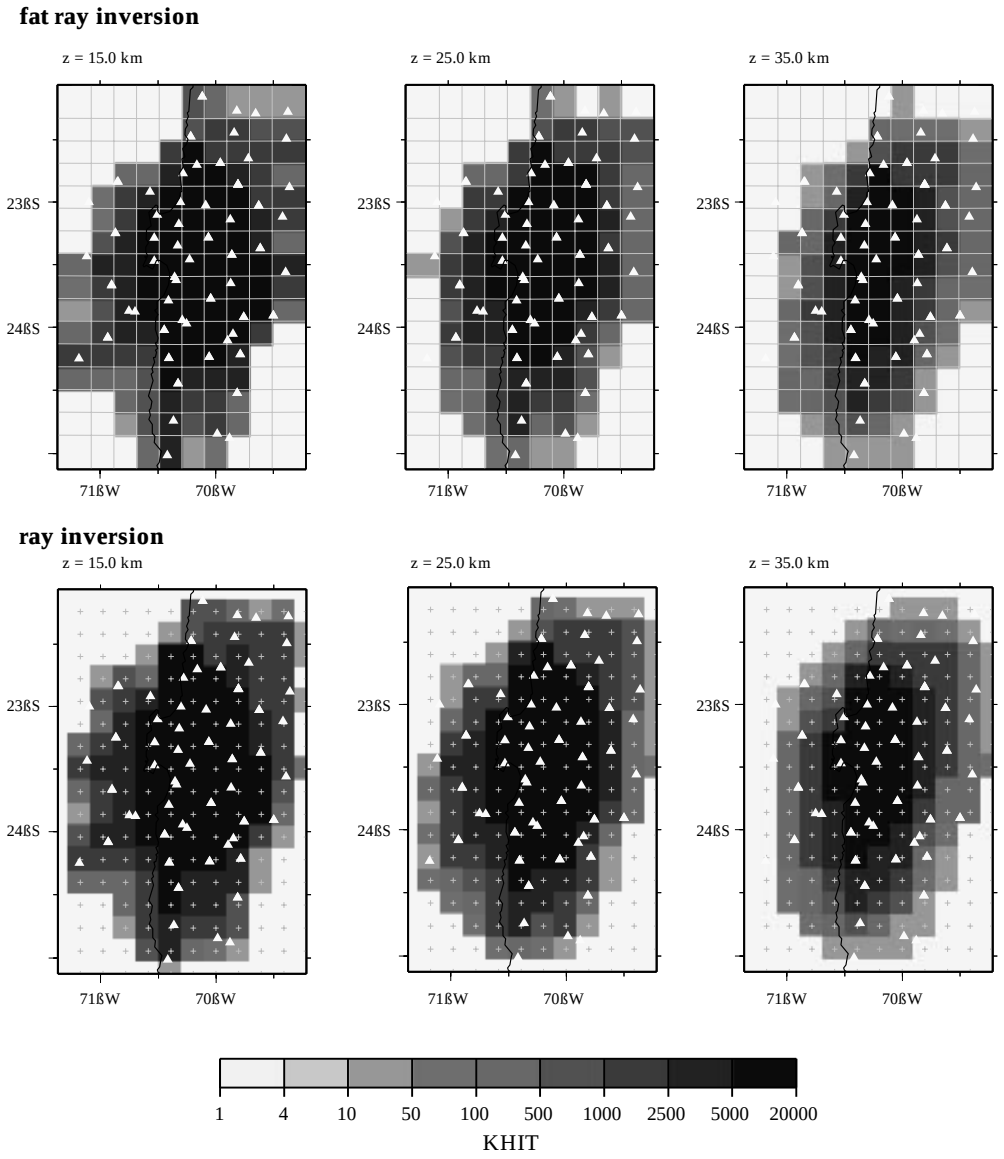

Fig. 12. KHIT for fat ray (top) and ray (bottom) of the inversion of the synthetic data obtained by using the source-receiver distribution shown in Fig. 10 and the synthetic model shown in Fig. 11. Grey lines mark inversion cells of fat ray tomography (top). Crosses in the ray tomographydenote grid points defining the inversion grid. Stations are marked by triangles.

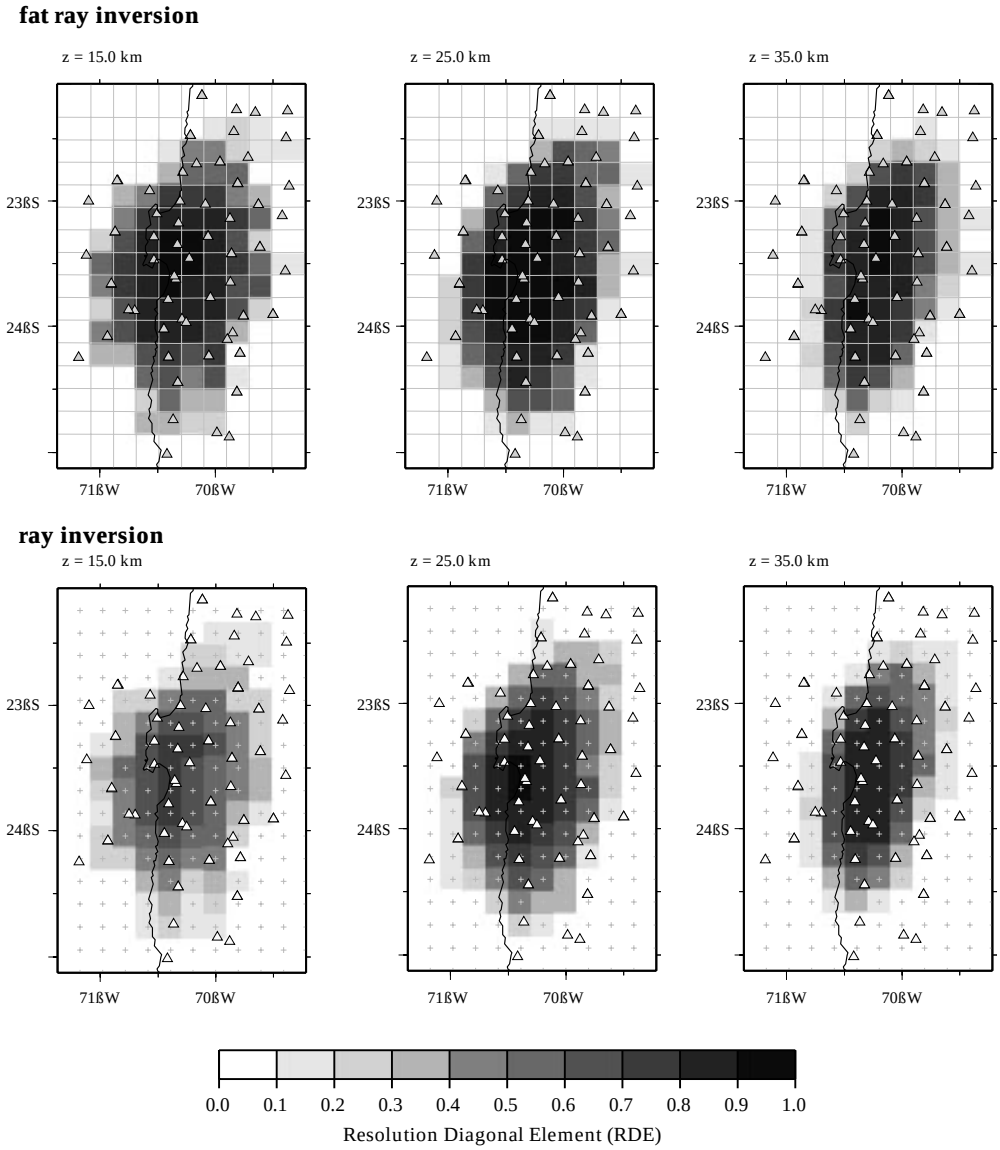

Fig. 13. RDE for fat ray (top) and ray (bottom) of the inversion of the synthetic data obtained by using the source-receiver distribution shown in Fig. 10 and the synthetic model shown in Fig. 11. Grey lines mark inversion cells of fat ray tomography (top). Crosses in the ray tomographydenote grid points defining the inversion grid. Stations are marked by triangles.

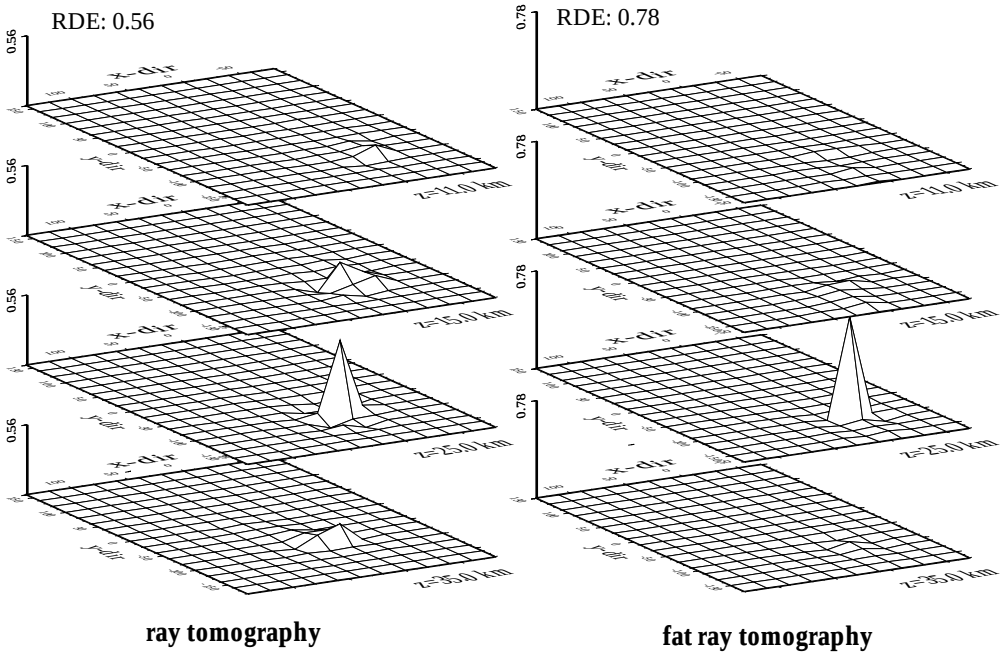

Fig. 14. 3-D plot of complete rows of the resolution matrix obtained by ray and fat ray tomography for a model parameter at 25.0 km depth. N larger smearing (i.e. higher off-diagonal elements) in the ray tomography.

amplitude recovery seen in the results obtained by fat ray tomography (Fig. 11), however, indicate lower model uncertainties for fat ray tomography.

Hypocenter locations obtained by ray tomography are significantly closer to the true hypocenter locations than the ones obtained by grid search implemented in fat ray tomography. Table 1 lists differences of hypocenter locations between true locations, as input, and those after 2 iterations of the synthetic data set obtained by fat ray and ray tomography. Hypocenter locations obtained by grid search in fat ray tomography are shifted on average by a distance corresponding to the grid spacing used in the fine grid search. Obviously, the grid search algorithm, as implemented in fat ray tomography, does not locate an earthquake on a point position as it is done when using rays, but rather within a volume which is defined by the numerical grid spacing.

Table 1:
Average and standard deviation of hypocenter differences between true and final hypocenter locations (after two coupled iterations) for fat ray and ray tomography

	Longitude (m)	Latitude (m)	Depth (m)	Origin time (ms)
Fat ray tomography				
Average	-1257	1147	1205	-66
S.D.	697	1013	2271	289
Ray tomography				
Average	6	-146	107	-0.3
S.D.	376	456	900	91

This limitation of hypocenter locations to a fixed volume yields higher RMS values for the hypocenter locations in fat ray tomography (Table 2). Having more hypocentral parameters (3200) than model parameters (940), the higher RMS values for the

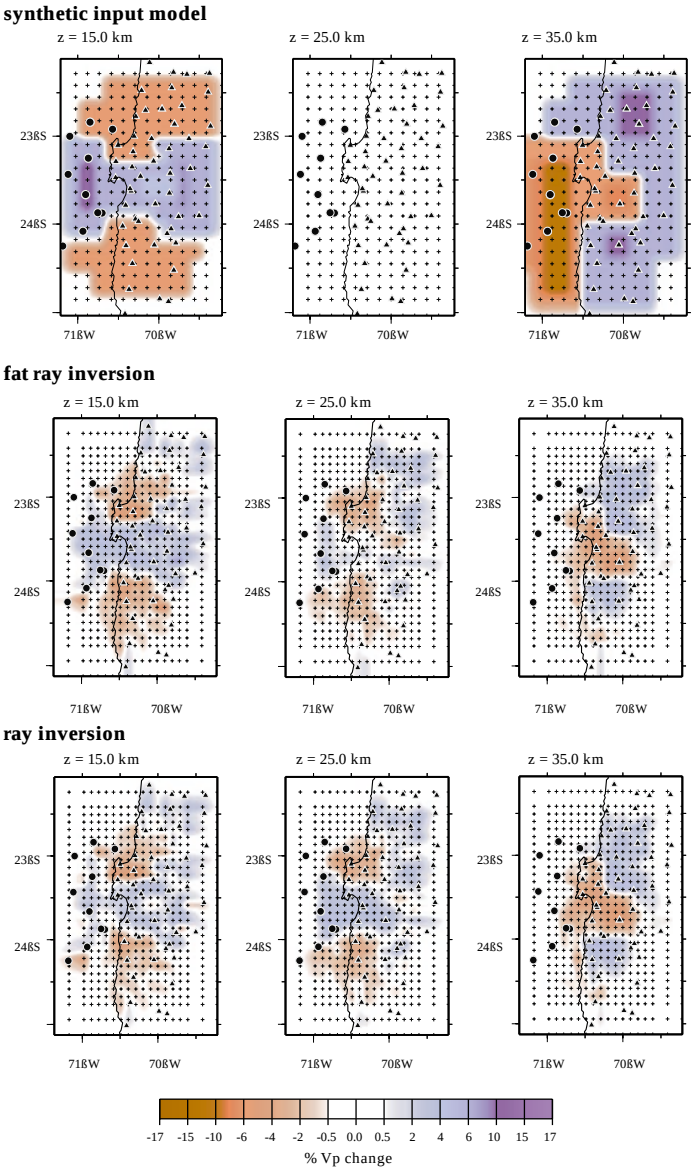

Fig. 15. Synthetic input model (top) and inversion results with reduced grid spacing after 2 iterations obtained by fat ray (middle) and ray inversion (bottom). Circles (offshore) and triangles mark stations (onshore). Crosses mark grid nodes defining velocities.

Table 2:
Initial and final data RMS and data variance, final average event RMS, and final model variance of the inversion of the synthetic CINCA dataset

	Initial data RMS (s)	Final data RMS (s)	Final average event RMS (s)
Fat ray tomography	0.191	0.166	0.076
Ray tomography	0.129	0.059	0.049
	Initial data variance (s^2)	Final data variance (s^2)	Final model variance (km^2/s^2)
Fat ray tomography	0.0363	0.0275	0.0056
Ray tomography	0.0167	0.0035	0.0069

hypocenter locations yield a significant higher final total (hypocenter and model) data RMS for fat ray tomography (Table 2). By choosing a smaller numerical grid spacing for the grid search algorithm, hypocenter locations are located closer to the position obtained by ray tomography and show smaller RMS values. By relocating mine blasts, however, the absolute error of the hypocenter locations of the CINCA data set has been determined as 1 km in epicenter and 2 km in focal depth (Husen et al., 1999), which is in the range of the chosen numerical grid spacing. Consequently, the difference in the final data RMS between ray and fat ray tomography is smaller than the real error imposed by the hypocenter locations and, therefore, not significant.

The results presented above emphasize the similarity of fat ray and ray tomography regarding inversion results and resolution estimates for the chosen model parameterization. To investigate the influence of model parameterization on fat ray and ray tomography, we performed a second synthetic inversion with the same setup but with a reduced grid node spacing of 10 km. With reduced grid spacing, fat ray tomography yields significantly better inversion results than ray tomography (Fig. 14). Especially at 15 km depth, where rays are travelling mostly subvertical, inversion results obtained by ray tomography are more patchy. This is obviously a result of finer model parameterization, which narrowed the influence volume of a ray. At greater depth, ray coverage is improved due to a higher number of events and similar results are achieved by fat ray and ray tomography. These results document that in areas of low resolution ray tomography is more sensitive to model parameterization than fat ray tomography. Designing the correct model parameterization is more critical in ray tomography.

6. Conclusions

In wave-equation tomography arrival times are no longer represented by first arrivals since scattered energy is delayed. In general they are picked by cross-correlation or at the maximum within the first half-cycle though the meaning of arrival times in applications of wave theory is still a matter of debate (see f.e. Williamson & Worthington, 1993). Finite-difference modelling of the eikonal equations is used in our approach to compute arrival times, which is still a high-frequency approximation. Hence, with regard to arrival times fat ray tomography corresponds with pure ray tomography and controlled-source seismology, and we use first arrivals as arrival times (f.e. Alan, 1982). The partial derivatives are computed using a Fresnel volume approximation.

Fréchet kernels or wavepaths show non-uniform sensitivity to velocity perturbations. Sensitivities are rather peaked at the source and the receiver and go to zero along the corresponding ray path (e.g. Vasco et al., 1995; Hung et al. 2000) whereas in our approach sensitivity is uniform within the fat ray. However, there may be a trade-off between theory (non-uniform sensitivity) and large-scale application in real earth such as local earthquake tomography. Peaked sensitivities at source and receiver would transfer uncertainties associated with source and site effects (unknown source time function, small-scale heterogeneities beneath the receiver, uncertainty in source and receiver position) into the model. In addition, for applications such as local earthquake tomography, where the recovered anomalies are significant larger than the wavelength, uniform sensitivity within the fat ray seems a justified first-order approximation (G. Nolet, 2000, personl communication). To investigate the influence of non-uniform sensitivity on the solu-

tion and resolution a carefully designed comparative study is needed using 3D Fréchet kernels as presented by Dahlen et al. (2000), which is beyond the scope of this paper.

In local earthquake tomography the coupling between hypocenter locations and seismic velocities demands the relocation of earthquakes during the inversion process. To extend the physical smoothing of Fresnel volumes from seismic velocities to hypocenter locations, we use a grid search algorithm to relocate the events. Thereby earthquake locations correspond to a volume, which is in our case defined by numerical grid spacing used for the FD calculations. The restriction of a hypocenter location to be within a volume has some implications on the event's data RMS and variance. They will be larger than those obtained for a point position. Despite this seemingly poorer performance in hypocenter locations, fat ray tomography for the coupled hypocenter-velocity problem yielded superior tomographic results than ray tomography. This documents that data RMS and variance improvements may be unreliable tools to judge the performance of inversion routines in some cases, especially in local earthquake tomography where equal or more numbers of hypocentral parameters exist than velocity parameters.

The results of our tests with synthetic data clearly showed the importance of the solution of the forward problem on inversion results and on resolution estimates such as KHIT and RDE. Our results, however, also revealed that effects of different model parameterizations are at least of the same order of magnitude as the effects resulting from different solutions of the forward problem. Ray tomography is more strongly affected than fat ray tomography by model parameterization. For finer model parameterization, fat ray tomography yields significantly better inversion results than ray tomography.

Our new approach to the solution of the forward problem in seismic tomography, called fat ray tomography, presents a step toward wave-equation tomography in large-scale applications such as local earthquake tomography.

Acknowledgements

We wish to thank Florian Haslinger for his fruitful contributions. The reviews of Cliff Thurber and an anonymous referee improved significantly the manuscript. This work was financially supported by the Swiss TOMOVES project BBW 97.0451 as part of the EU research project Enviroment ENV4-CT98-0698. This contribution number 1143 of the Institute of Geophysics, ETH Zurich.

References

Allen, R., 1982. Automatic phase pickers: Their present use and future prospects. Bull. Seism. Soc. Am. 72, 8225-8242.

Cardimona, S. and Garmany, J., 1993. Smoothing operators for waveform tomographic imaging. Geophysics 58, 1646-1654.

Cerveny, V., and Soares, J.E.P., 1992. Fresnel volume ray tracing. Geophysics 57, 902-915.

Dahlen, F.A., Hung, S.-H., and Nolet, G., 2000. Fréchet kernels for finite-frequency traveltimes – I. Theory. Geophys. J. Int. 141, 157-174.

Eberhart-Phillips, D., 1986. Three-dimensional velocity structure in northern California Coast Range from inversion of local earthquake arrivel times. Bull. Seismol. Soc. Am. 76, 1025-1052.

Eberhart-Phillips, D., 1990. Three-dimensional P and S velocity structure in the Coalinga region, California. J.Geophys.Res. 95, 15343-15363.

Evans, J.R., D. Eberhart-Phillips, C.H. Thurber, 1994. User's manual for SIMULPS12 for imaging Vp and Vp/Vs: a derivative of the "Thurber" tomographic inversion SIMUL3 for local earthquakes and explosions. Open-file Report 94-431, U.S. Geological Survey, 101 pp.

Gelchinsky, B., 1985. The formulae for the calculation of the Fresnel zones or volumes. J. Geophys. 57, 33-42.

Ghose, S., Hamburger, M.W., Virieux, J., 1998. Three-dimensional velocity structure and earthquake locations beneath the northern Tien Shan of Kyrgyzstan, central Asia. J. Geophys. Res. 103, 2725-2748.

Hagedoorn, J.G., 1954. A process of seismic reflection interpretation. Geophysical Prospecting 2, 85-127.

Haslinger, F., 1999. Velocity structure and seismotectonics of northwestern Greece beween the Gulf of Arta and Zakynthos. Ph.D. Thesis ETH No. 12966, ETH-Zurich, pp. 159.

Haslinger, F., Kissling, E., Ansorge, J., Hatzfeld, D., Papadimitriou, E., Karakostas, V., Makropoulos, K., Kahle, H.-G., and Peter, Y., 1999. 3D crustal structure form local earthquake tomography around the Gulf of Arta (Ionian region, NW Greece). Tectonophysics 304, 210-218.

Hole, J,A., 1992. Nonlinear high-resolution three-dimensional seismic travel time tomography. J. Geophys. Res. 97, 6553-6562.

Hole, J.A., and Zelt, B.C., 1995. 3-D finte-difference reflection traveltimes. Geophys. J. Int. 121, 427-434.Hung, S.-H., Dahlen,

F.A., and Nolet, G., 2000. Fréchet kernels for finite-frequency traveltimes – II. Examples. Geophys. J. Int. 141, 175-203.

Husen, S., 1999. Local earthquake tomography of a convergent margin, north Chile. Ph.D. Thesis, Christian-Albrechts University Kiel, Germany.

Husen, S., Kissling E., Flueh, E., and Asch, G.,1999. Accurate hypocenter determination in the seismogenic zone of the subducting Nazca plate in north Chile using a combined on-/offshore network. Geophys. J. Int 138, 687-701.

Husen, S. and Kissling, E., 2000. Local earthquake tomography of shallow subduction in north Chile: a combined on- and offshore study. J. Geophys. Res. in press.

Kissling, E., Ellsworth W.L., Eberhart-Phillips D., and Kradolfer U., 1994. Initial reference models in local earthquake tomography. J. Geophys. Res. 99, 19,635-19646.

Kissling, E., S. Husen, and F. Haslinger, 2000. Model parameterization in seismic tomography: a choice of consequences for the solution quality. Phys. Earth. Planet. Interiors this issue.

Klimes, L., and Kvasnicka, M., 1994. 3-D network ray tracing. Geophys. J. Int. 116, 726-738.

Le Meur, H., Virieux ,J., and Podvin, P., 1997. Seismic tomography of the Gulf of Corinth: a comparison of methods. Ann. Geofis. 40, 1-24.

Luo, Y. and Schuster, G.T., 1991. Wave-equation traveltime inversion. Geophysics 56, 645-653.

Marquering, H., Dahlen, F.A., and Nolet, G., 1999. Three-dimensional sensitivity kernels for finite-frequency traveltimes: the banana-doughnut paradox. Geophys. J. Int. 137, 805-815.

Nelson, G.D., and Vidale, J.E., 1990. Earthquake locations by 3-D finite-difference travel times. Bull. Seismol. Soc. Am. 80, 395-410.

Podvin, P., and Lecomte, I., 1991. Finite difference computation of travel times in very contrasted velocity models: a massively parallel approach and its associated tools. Geophys. J. Int. 105, 271-284.

Pulliam, J., and Snieder, R., 1998. Ray pertubation theory, dynamic ray tracing and the determination of Fresnel zones. Geophys. J. Int. 135, 463-469.

Sambridge, M.S., and Kenett, B.L.N., 1986. A novel method of hypocenter location. Geophys. J. R. astr. Soc. 87, 679-697.

Stark, P.B. and Nikolayev, D.I., 1993. Toward tubular tomography. J. Geophys. Res. 98, 8095-8106.

Thurber, C.H., 1983. Earthquake locations and three-dimensional crustal structure in the Coyote Lake area, central California. J. Geophys. Res. 88, 8226-8236.

Um, J., and Thurber, C.H., 1987. A fast algorithm for two-point seismic ray tracing. Bull. Seismol. Soc. Am. 77, 972-986.

Vasco, D.W., and Majer, E.L., 1993. Wavepath traveltime tomography. Geophys. J. Int. 115, 1055-1069.

Vasco, D.W., Peterson, J.E., and Majer, E.L., 1995. Beyond ray tomography: wavepaths and Fresnel volumes. Geophysics 60, 1790-1804.

Vidale, J.E., 1988. Finte-difference travel time calculation. Bull. Seismol. Soc. Am. 78, 2062-2076.

Vidale, J.E., 1990. Finite-difference calculations of travel times in three dimensions. Geophysics 55, 521-526.

Virieux, J., 1991. Fast and accurate ray tracing by Hamiltonian perturbation. J. Geophys. Res. 96, 579-594.

Virieux, J., and Farra, V., 1991. Ray tracing in 3-D complex isotropic media: An analysis of the problem. Geophysics 56, 2057-2069.

Woodward, M.J., 1992. Wave-equation tomography. Geophysics 57, 15-26.